NRIAG Journal of Astronomy and Geophysics 6 (2017) 395–407

Contents lists available at ScienceDirect

NRIAG Journal of Astronomy and Geophysics

journal homepage: www.elsevier.com/locate/nrjag

Full length article

Mapping palaeolakes in the Ténéré Desert of northeastern Niger using space-borne data for groundwater potential

Gloria Molina [a], Ahmed Gaber [b,*], Farouk El-Baz [a]

[a] Center for Remote Sensing, Boston University, Boston, MA, USA
[b] Geology Department, Port-Said University, Port-Said, Egypt

ARTICLE INFO

Article history:
Received 29 August 2017
Revised 27 September 2017
Accepted 1 October 2017
Available online 7 October 2017

Keywords:
DEMs
Optical and radar images
Palaeolakes
Groundwater

ABSTRACT

Groundwater resources in arid lands are crucial for supporting life. Thus, delineation of low land areas, where surface runoff accumulated during pluvial periods assists in groundwater explorations. Therefore, the drainage patterns in northeastern Niger using various sources of DEMs of optical (ASTER) and radar (SRTM) satellite data were extracted. These data reveal three palaeolakes in the Ténéré Desert. In addition, the DEMs together with the optical and radar satellite data were used to define a major watershed measuring 634,000 km^2. This watershed may have led to the formation of one major palaeolake as an ancestor of the three palaeolakes. The latter extend to 11,514 km^2, 17,571 km^2 and 18,453 km^2. The optical and radar satellites images show that the boundaries of these three lakes have been modified by extensive longitudinal and transverse sand dunes of considerable thickness. These dunes accumulated during a much later arid episode in geologic time, probably during the late Quaternary. Prior to that, the former marshlands received water from the Tibesti Mountains of northern Chad, the Ahaggar Plateau of southeastern Algeria and the Air Mountain of northern Niger. The drainage patterns clearly show the pathway of water down to the ground level. The longest drainage line is emanating from the Ahaggar Plateau and extends south west for 837 km. The water overflow of the southernmost lake led to the formation of another distinct drainage line, leading to the southwestern edge of the ancestral Megalake Chad. This drainage line begins in the vicinity of the town of Fachi and extends southward through the town of Dillia as a single tributary, and is here named the Dillia Palaeoriver. These observations, which are based on the study of satellite data require geophysical fieldwork to ascertain the interpretations, and evaluate the potential for groundwater accumulation in the region.

1. Introduction

In arid and semi-arid regions, groundwater resources are crucial sources for life and economic development. Recent climate models predict an increase in aridity in the coming decades for most of Africa, among other regions (Dai, 2011). Thus, persistent droughts will likely cause water shortages, particularly in North Africa. Over the past forty years, Niger has experienced seven episodes of drought with dramatic consequences on agro-pastoral production, food security and socio-economic (African Development Bank, 2012). Meanwhile, the groundwater along within desert areas is considered as a good alternative resource, where the surface water is limited or totally absent. However, mining these fossil groundwater reserves should be considered in a planned manner by providing scientific information about the quantity and quality.

Meanwhile space-borne imaging using various electromagnetic wavelengths (visible, infrared and microwave) is an effective method for exploring large and inaccessible areas in a bird eye view by providing geomorphological, hydrological, and geological data. Radar remote sensing, in particular represents a valuable source of information to complement those imaged by visible and infrared sensors. Radar waves have the capability to penetrate dry sands and reveal information on the dielectric and geometric properties of the surface and near-surface. Many authors reported that space-borne SAR can penetrate the sand surface and show

* Corresponding author.
E-mail address: ahmedgaber_881@hotmail.com (A. Gaber).
Peer review under responsibility of National Research Institute of Astronomy and Geophysics.

Production and hosting by Elsevier

https://doi.org/10.1016/j.nrjag.2017.10.001
2090-9977/

hidden paleo-hydrological and tectonic structures, where the low frequency radar signal allows access to subsurface information down to a depth of a few meters (El-Baz, 1998; Paillou et al., 2003; Robinson et al., 2006; Gaber et al., 2015; Skonieczny et al., 2015; Paillou, 2017).

The land surface features of the Ténéré Desert of Niger represent an example of the vast dry eastern Sahara. It is known from previous studies that the Great Sahara hosted humid periods in the past. According to Tierney et al. (2017), the Great Sahara had 10 times the amount of rainfall as it receives nowadays. However, today rainfall in the Sahara ranges from 4 inches to less than 1 inch per year. The African humid period of the early Holocene to mid-Holocene fluctuated from abundant rainfall and rich biodiversity to dry conditions (Skinner and Poulsen, 2016). Six thousand years ago, the Great Sahara was green and covered by trees, lakes, rivers, savannah fauna, annual grasses and much rainfall (Jolly et al., 1998; Gasse, 2000; Drake et al., 2011; Boos and Korty, 2016). However, climate changes transformed the green region into dry lands (Tierney et al., 2017). This transition was related to a shift in the circulation of the tropical atmosphere (Boos and Korty, 2016).

Evidences that the Great Sahara was a wet region were presented in several studies, where researchers have discovered the existence of prehistoric megalakes and palaeorivers buried beneath the sand through the study of satellite images, including radar images (eg. Robinson et al., 2000; Ghoneim and El-Baz, 2007; Ghoneim et al., 2007; Gaber et al., 2009; Maxwell et al., 2010; Larrasoaña et al., 2013). At the present times the region has limited rainfalls and its land surface is reshaped by the prevailing wind (Fabre and Mainguet, 1991; Goudie, 2002; El-Baz, 1998; Brookfield, 2011). The wind affects the landforms in all climates, however, for significant effects, it needs to be strong enough to erode and transport sediments with the absence of vegetation cover (Shao, 2001). The region of northeastern Niger (Fig. 1) has been selected as an example of a non-vegetated and dry area of the eastern Sahara to reveal its ancient landforms using available satellite images.

The selected study region is considered one of the largest protected sanctuaries of Saharo-Sahlien wildlife areas in Africa. It covers over 7.7 million hectares, which include the Air mountains and a small Sahelian pocket (Lockwood et al., 2006). Most of the study area is covered by aeolian sand in the form of an undulating sand sheet (Warren, 1971). It comprises a vast plain of sand stretching from northeastern Niger into western Chad. The Air Mountain borders the area to the west. It is a triangular crystalline volcanic massif and sedimentary rocks ranging in age from the Precambrian to Cenozoic (Choubert et al., 1987). The Ahaggar, and the Tassili-in-Ajjer Mountains bound the study area to the north. To the east, the area is bounded by the Tibesti massif of northern Chad (Fig. 1). The southeastern side of the study area is characterized by a concentration of sand sheets that were mapped by Mainguet and Callot (1978). There, the dunes are spatially oriented in longitudinal and transverse forms. The transverse sand dunes form the Erg of Bilma; which stretches southwest from Dillia and the Tibesti Mountains (Rossi and Marinangeli, 2004). Based on the study of the Niger geology by the British Geological Survey (BGS) and the U.S Geological Survey (USGS), the study area is dominated by the sedimentary Cretaceous-Tertiary-Chad Basin (Fig. 2) (Persits et al., 2002).

The northeastern part of Niger is an arid region with vast accumulations of sand. It is well known for its sand dunes and sand

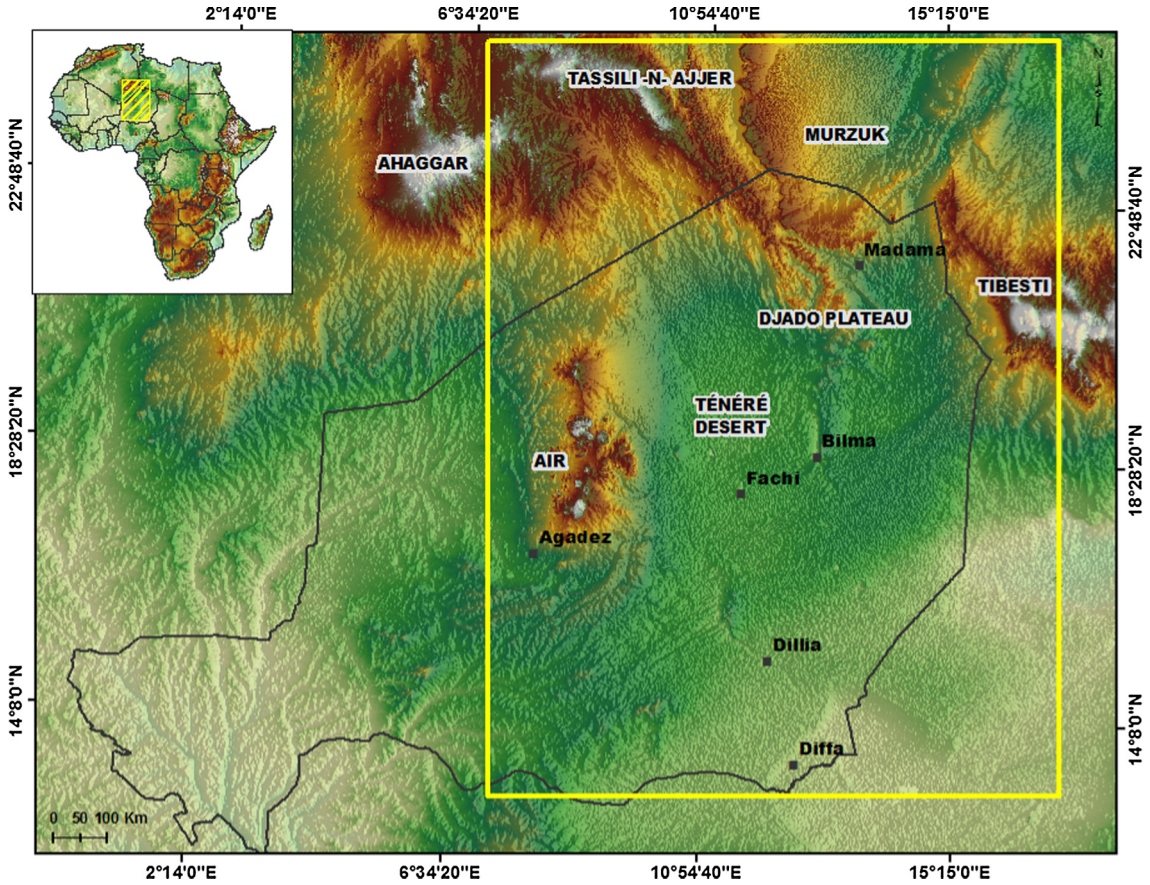

Fig. 1. SRTM topography, covering most of the eastern segment of Niger in North Africa. Study area is represented by the yellow box, while the black line is the political boundary of Niger.

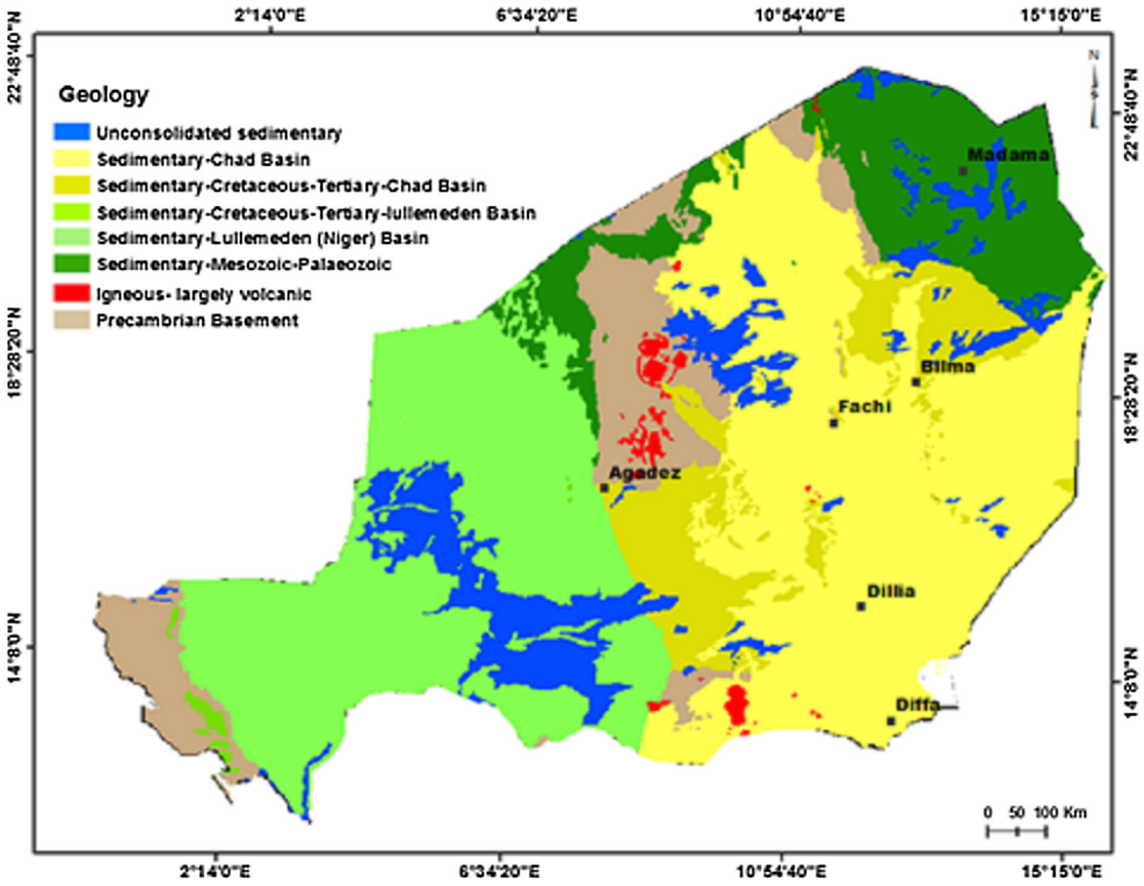

Fig. 2. Geologic map of the Niger from the British Geological Survey and the United States Geological Survey in 1964 and scale 1:5 million (USGS).

sheets, where at least 20% of its total surface area is covered by sand (Wilson, 1973). This condition is much like the rest of the deserts in North Africa, Arabia and Australia. These Lands lie between (15–30° N and 15–30° S), and are similar to those of mid-latitudes in central Asia, and the semiarid great plains of North America. The formation and accumulation of sand seas and dunes are controlled by the amount of sand supply and the directions of the prevailing winds. In Niger, the wind pattern is basically from east to west, similar to the rest of the central Sahara (Mainguet and Callot, 1978). In Niger, the sand seas occur on all sides of the central uplands and move from the eastern to the central parts of the desert to form thick accumulation of sand (Mainguet and Chemin, 1983).

The purpose of this study is to utilize all available satellite images (optical, thermal, radar and DEMs) to map the surface and near-surface features in the area and define the paleodrainage patterns and their later covering by windblown sand. It is obvious that this region hosted a great amount of accumulated surface water runoff in the past, thus its geomorphology was totally different from its current situation.

2. Dataset and Methods

2.1. Characteristics of the used dataset

Satellite data were utilized in this study to extract the hydrogeological features and other water-related land surface properties. Several types of satellite-derived data were used for modeling runoff processes, locating recharge areas and predicting the water flow and accumulation regions. Satellite-derived products includes digital elevation models, landforms, geologic structures, surface lithology, rainfall distribution and rate, as well as surface temperature anomalies. The entire study area was mapped using satellite images from a variety of sensors with different spectral, spatial, and temporal characteristics.

For the optical data, the Landsat-8 and Sentinel-2 images were used. Landsat-8 was launched on February, 2013 as part of the Landsat Data Continuity Mission. It operates in two main sensors, the Operational Land Imager (OLI) and the Thermal Infrared Sensor (TIRS). The OLI sensor uses nine spectral bands with 30 m spatial resolution and the panchromatic band with 15 m spatial resolution. While, the TIRS consist of two thermal bands, 10 and 11. These bands were collected at 100 m spatial resolution and resampled to 30 m. In addition, Sentinel-2 optical data were used for visual interpretation. The Sentinel-2 mission conducts monitoring by two satellites and provides high resolution optical imagery at 10, 20 and 60 m spatial resolutions. In the present study the bands 2, 3, 4 and 8 of Sentinel-2 with 10 m spatial resolution acquired in 2017 were used as well as the multispectral, thermal and panchromatic bands of Landsat-8 data acquired in 2016 and 2017.

In this study we used the DEMs produced by ASTER stereo images as well as by interferometric synthetic aperture radar (SAR) systems, such as the one produced by the Shuttle Radar Topography Mission (SRTM) flown in February 2000. ASTER stereo and STRM data allowed the production of seamless and consistent DEM mosaics of the entire study area at the scale 1:50,000. ASTER DEMs were produced at 15 m and averaged to 30 m. Although the original resolution of the SRTM DEM was 90 m, the data was processed at 30 m resolution. Both DEM data sets were used to extract basin morphometric parameters and evaluate their usefulness as input parameters in regional hydrologic models. For example, the

SRTM data reflect palaeotopography in the flat desert areas (Schaber et al., 1997; Robinson et al., 2006; Ghoneim and El-Baz, 2007; Elmahdy and Mohamed, 2013). The SRTM instrument consists of the Spaceborne Imagine Radar C-band (SIR-C) and has the capability to penetrate the well sorted and very dry sand sheets (Kobrick, 2006).

This data is one of the most widely used elevation product (Luedeling et al., 2007; Elmahdy, 2011). However flat regions present gaps in areas of low radar backscatter (Nikolakopoulos et al., 2006; Hirt et al., 2010). Another DEM was created from ASTER Global Terrain Model (ASTGTM), V2 (NASA JPL, 2013), to evaluate if the surface features differ from those in SRTM data. The improvements of these data include decrease in voids in areas that appear relatively flat by a new water detection algorithm, where the artifacts are mostly disappeared (ASTER, 2011).

Radar data allow mapping and characterizing surface and near-surface features such as palaeodrainage and fractures hidden by aeolian sand or fluvial deposits. It is an optimal sensor when used with multiple frequencies and polarization modes. We made ample use of the ALOS/PALSAR-1 and Sentinel-1 images with different frequencies (L- and C-band). Thus, to map the near-surface features, the L-band radar ALOS/PALSAR-1, data from Global Palsar-1/Palsar/JERS-1 mosaic with 25 m spatial resolution acquired in 2010 as well as the Sentinel-1 were used. These radar data are ortho and slope corrected for backscattering coefficient with horizontal and vertical polarization (HH and HV). Moreover, to identify the near-surface features, the Sentinel-1 radar data acquired in May 2017 with its C-band and dual polarization (VH and VV) from Copernicus (https://scihub.copernicus.eu/dhus/#/home) was utilized. Ancillary data included, geological maps, daily precipitation data from weather data from Tibesti meteorological station (in Chad) as well as the daily averages maps from Tropical Rainfall Measuring Mission (TRMM) data were used. In this work, the precipitation data were correlated with the thermal data.

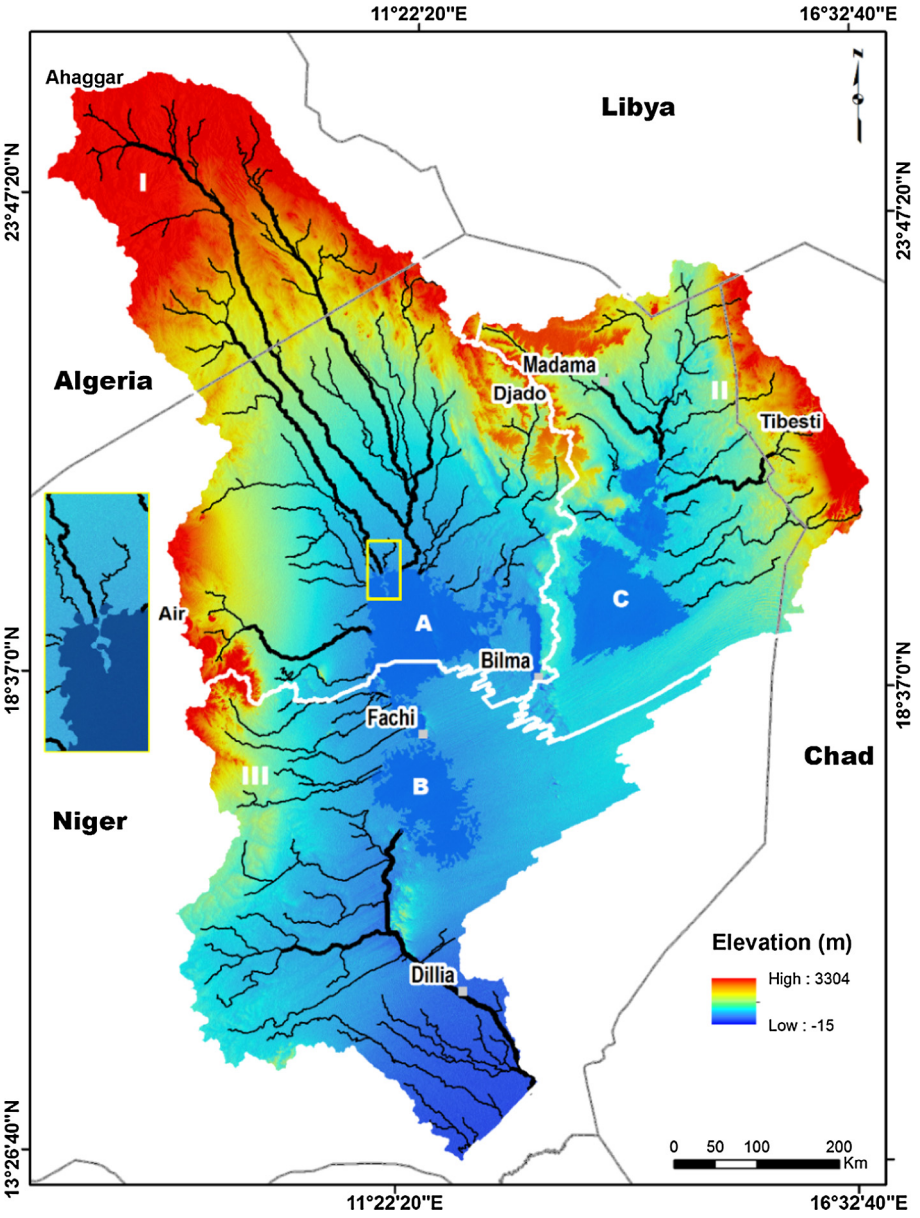

Fig. 3. SRTM mosaic showing the basin and drainage patterns from the Ahaggar Mountain of southern Algeria, to the northwest and Djado plateau in the north, Tibesti Mountain to the east and the Air Mountain in the West. The three visible flat areas (A, B and C) could have been a large marsh during times of plentiful rainfall in the geological past. The total drainage may have led water to the straight segment in the bottom to the ancestral Megalake Chad. Sub-basins are marked in white lines. Yellow box shows the area of enlargement to the left, which indicates a promontory from a distinct drainage line in the Megalake Chad.

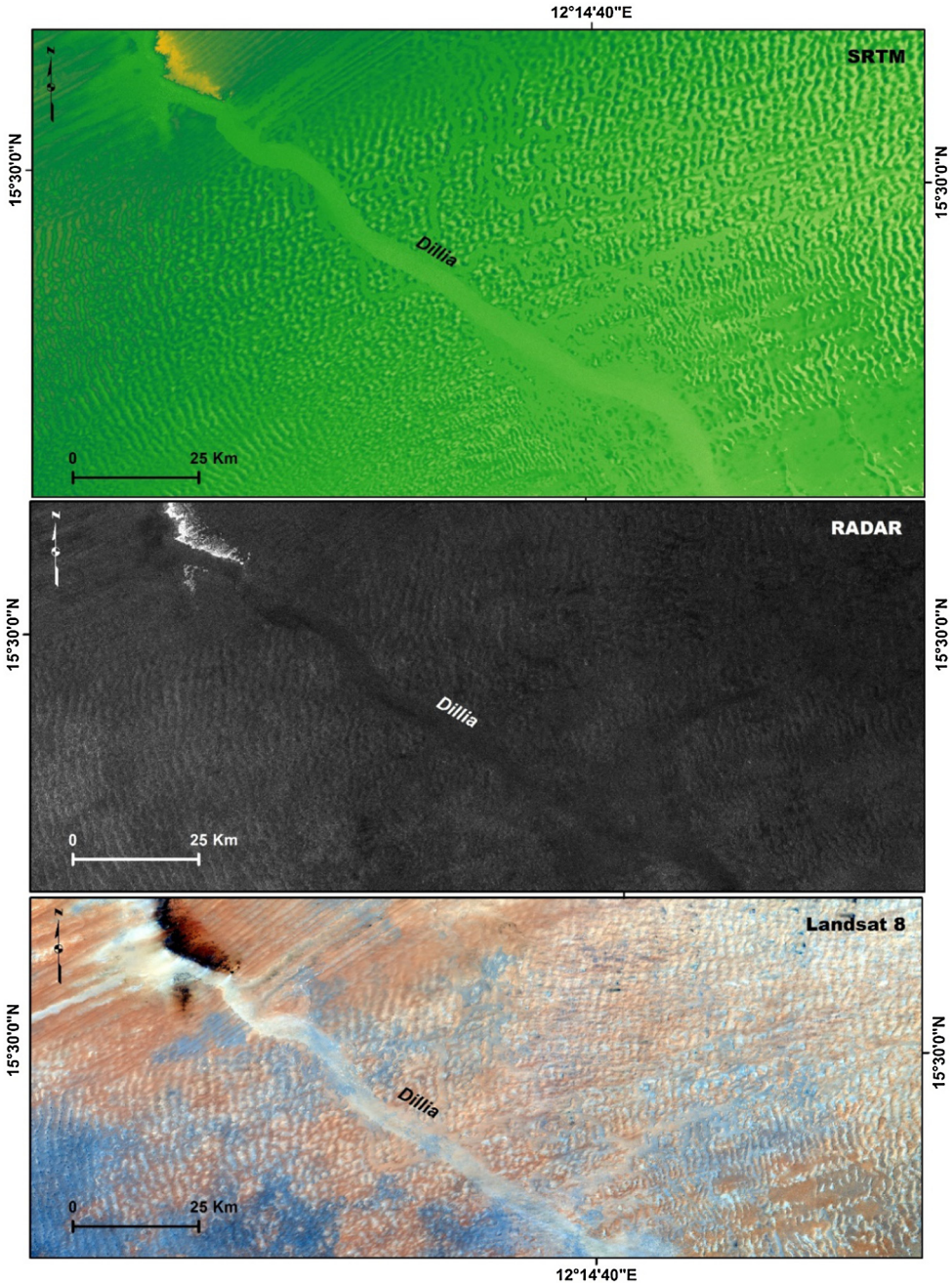

Fig. 4. SRTM at top clearly showing the drainage line, named the Dillia Palaeoriver, leading to the western edge of Megalake Chad. Radar ALOS/PALSAR data in the middle also show the drainage line in a dark tone and Landsat 8 at the bottom shows this line in a light tone due to its sandy soil.

2.2. Processing

Digital elevation models (DEMs) of the SRTM and ASTER were created and transformed into the same projection, Universal Transverse Mercator (UTM), zone 32, WGS 1984 Datum to extract the surface drainages network. The models cover the study area and all of its watersheds. The elevation void fill function was applied to eliminate the voids in the data. These voids occur when no data were collected within the area represented by a pixel, mostly in flat level terrain. These voids need to be eliminated; otherwise they would affect the accuracy of the hydrological results, creating run-off interruption (Tarboton, 1997). After removing the voids, the eight directions model (D8), which was first introduced by O'Callaghan and Mark (1984), was performed. This algorithm determines the direction of flow from every cell in a given DEM assigning flow from each pixel to one of its eight neighbors, either adjacent or diagonal, in the direction with steepest downward slope. This has been widely used to delineate drainage networks (Marks et al., 1984; Jenson and Dominque, 1988; Fairfield and Leymarie, 1991; Martz and Garbrecht, 1992; Costa-Cabral and Burges, 1994; Tarboton, 1997; Ghoneim and El-Baz, 2007; Ghoneim et al., 2002; Elmahdy and Mohamed, 2013). However using this widely used method in flat areas where gaps exist is a great challenge (Zhao et al., 2009).

Following the flow direction, the flow accumulation was calculated, which gives the flow as the accumulated weigh of all cells flowing into each downslope cell. Basically, the value in each cell contains the sum of the amount of water that fell on all the raster

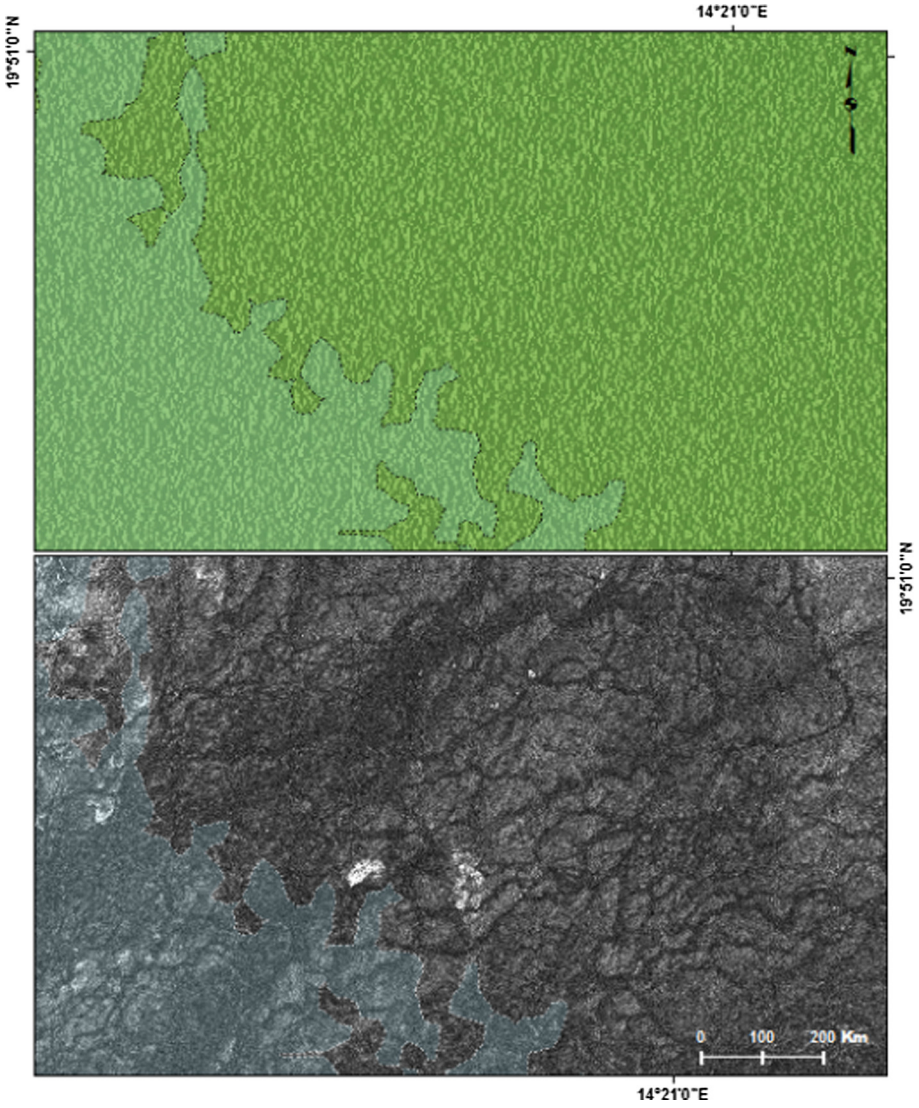

Fig. 5. The SRTM (top) showing slight differences in the topography than the Radar Sentinel-1 (Bottom). Paleochannels show up clearly in the radar Sentinel-1 image and indicate water flow from northeast to southwest. These channels are covered by sand in the SRTM iamge.

cells upstream from it. However, the flow accumulation performed in ArcGIS 10 presented a limitation, and did not work on both positive and negative values. This issue was resolved in the ArcGIS 10.1 version (Dilts, 2015). Streams were defined after the flow accumulation step, using a threshold of 5000 cells. These procedures were performed on both the SRTM and ASTER data. Both elevation data were chosen to compare the delineation of streams network. Drainages were slightly edited in the flat areas where streams lead to straight lines across lakes. Delineation of the borders of the palaeolakes was done where streams rimmed the edges of the palaeolakes along the same contour lines. These were manually filled at elevation of 414 and 457 m. amsl., which is the maximum elevation of the corresponding lakes. The resulting drainage network was overlaid on the other satellite data to validate the algorithm result. The main watershed was then delineated and vectorized for spatial analyses.

For visual interpretation and validation, optical and radar data were taken into consideration. In this context, Landsat-8 data provided visual details of the surface features, and thermal bands 10 and 11 were used to detect the anomalies. These bands were radiometrically calibrated using ENVI 5.3 version to obtain brightness temperatures. Several Landsat-8 scenes covering the study area were selected from January to December 2016, to examine the temperature behavior during a year and visually detect any anomaly. Moreover, Sentinel-2 optical data with 10 m spatial resolution were mosaicked to visually detect any different features and compare them with the Landsat-8 images. In addition, the radar data (ALOS/PALSAR-1 and Sentinel-1) of the entire study area were calibrated, filtered, geocoded and mosaicked for different polarization modes (HH, VV and HV). This was done to detect the near-surface features and the palaeolakes extensions, which are buried under the sand deposits and are not visible in other data.

3. Results

The generated topographic data from the DEMs (Fig. 3) show the routes of the drainages patterns from the higher (upstream) to the lower elevations (downstream). By comparing the obtained results using ASTER/DEM data with the SRTM/DEM, the SRTM data gave better hydrological results specialty in the flat areas. Previous comparisons reveal that the SRTM/DEM presented better vertical accuracy than the ASTER/DEM (Hensley et al., 2001; Fujisada et al., 2005; Slater et al., 2009; Forkuor and Maathuis, 2012). The main tributaries emanate from the Ahaggar and Tassili-in-Ajjer

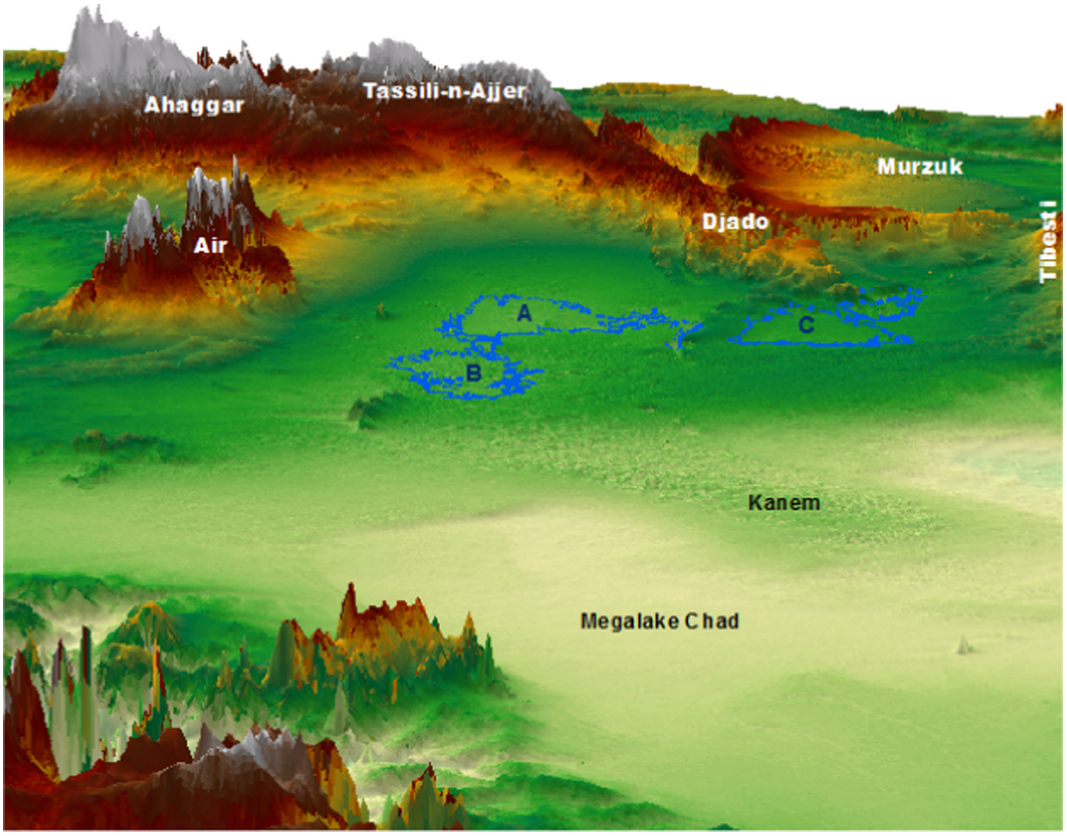

Fig. 6. 3D map showing topographic variations in the study area. The highest elevations of Ahaggar, Air and Djado Plateau are represented in dark and light tones, while flat areas are depicted in shades of green. The outlines of the three palaeolakes are shown in light blue lines. The yellowish green shows low flat areas, which correspond to the ancestral Megalake Chad.

Mountains of southeastern Algeria at average elevation of 900 m, where the longest drainage line extends to the length of 837 km. Some tributaries emerge from the west at the Air Mountain, which is up to 1800 m high. Other tributaries emerge from the Tibesti Mountains of northern Chad, and Djado plateau and Murzuk basin of southern Libya. In the southernmost part of the drainage basin extends a singular drainage line, which is observed in both optical and radar satellite images. This distinct drainage line begins in the vicinity of the town of Fachi and extends southward as a single tributary. As it passes by the town of Dillia, it is here named the Dillia Palaeoriver. It further leads to the southwestern edge of the ancestral Mega Lake Chad (Fig. 4). This distinct drainage line must have been an important contributor to Lake Chad during rainy periods.

In addition, topographic data of the study area reveals the interruption of the drainage patterns in the southern part of Niger by considerably thick deposit of sand dunes. Because of the capability of radar data to penetrate the dry sand sheets, some channels were observed near the boundaries at the lower topographic areas (Fig. 5). Moreover, several drainage patterns emerge from Djado Plateau were revealed in radar data, but were not visible neither in the SRTM nor optical data (Fig. 5). Although the flat regions are covered by considerable amounts of sand, some promontories are visible in the satellite image data. For example the SRTM data show a delta deposit at the end of the drainage pattern leading to the lake (enlargement in Fig. 3).

The total watershed of the region, occupies an area of about 634,000 km^2, which corresponds to 25% of the entire Chad basin, which measures 2,454,081 km^2. It represents a major basin that must have led to the much larger sub-basin of Megalake Chad. The latter is one of the largest sedimentary basins in Africa and considered to overlay a large subsurface aquifer (Leblanc et al., 2007). The eastern boundaries of this sub-basin are dissected by the blown sand dunes deposits. These sand dunes have different shapes and thickness depending on the directions of the prevailing wind and the amount of available sands (Mainguet, 1978, 1984).

From the processed satellite images, it was possible to divide the basin into three sub-basins. The one in the northeast is pear-shaped and covers an area about 154,804 km^2. The basin in the north is considered the largest one and measures an area about 278,604 km^2 and it is also pear-shaped, but in the opposite direction. The basin in the south covers about 201,233 km^2 and is more irregular and not fully defined, due to sand dune accumulations. It is obvious that the sand dunes have completely masked the eastern boundaries of the three sub-basins. The flatness of the terrain at the end of the drainage patterns within the three sub-basins is clearly depicted in the satellite image data (Fig. 3). It is most appropriate to assume that these flat surfaces represent lake deposits from the drainage patterns. Therefore, it is conceivable that these flat and sand covered areas would have higher potential for groundwater accumulations, and are recommended for hydrogeophysical explorations.

In this study, a major basin of approximately 140,000 km^2 was defined, which today can be separated into three distinct palaeolakes. The southernmost part of these palaeolakes was the source of a single tributary (named Dillia Palaeoriver), which appears to have led to the south western edge of the former Megalake of Chad. The boundaries of these lakes have been modified by later events, particularly by the windblown deposits of thick sand dunes accumulation. The thickness of the sand dunes in the study area has been described by some researchers of the Sahara and the Sahel using the sand budget method (Mainguet and Chemin, 1983). This

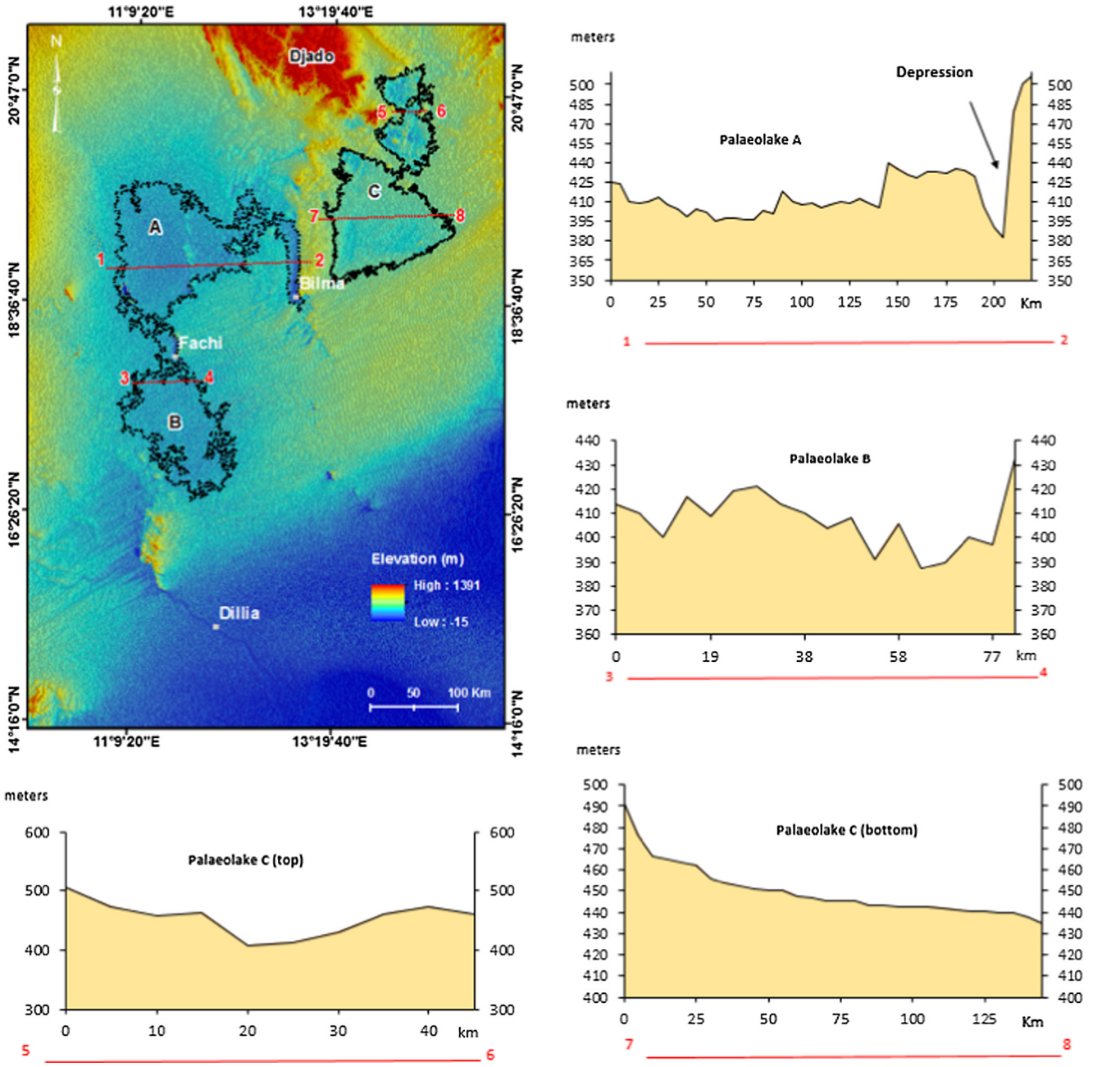

Fig. 7. DEM topography showing the locations of the cross sections in red lines. Palaeolakes (A) and (B) show relatively flat areas with pronounced depression along the profile. In that major depression several villages are located close to groundwater resource. Paleolake (C) presents relatively flat topography.

method includes two parameters, transportation and deposition, in which the interaction of the amount of sand in and out of a sand sea determines the thickness of the accumulations.

The study area ranges from the high altitudes of Ahaggar, Air and Djado plateau and Tibesti Mountains to flat areas, which includes the Kanem region that is characterized by sand dunes deposits in the form of transverse dunes reaching heights up top 60 m (Mainguet and Chemin, 1983). The northern side of the Kanem region is characterized by the prevalence of sand dunes and the absence of surface water (Vassolo, 2012).

4. Discussion

The obtained results clearly display the location of three distinct flat areas, which are interpreted as palaeolakes (Figs. 3 and 6). The one on the east (C) was fed from the Tibesti Maintains and the southern boundaries of Murzuk basin in Libya, and in part, from the terminal Ahaggar mountains. To the west of palaeolake C, lake (A) was fed by the major drainage patterns that emanated from the higher reaches of the Ahaggar mountains of southeastern Algeria. The southernmost lake (B) was fed by the Air Mountains of the central Niger. The eastern boundaries of the palaeolakes are not clearly visible because of the geologically younger sand deposits.

The total surface areas of these palaeolakes (A, B & C) are 11,514 km^2, 17,571 km^2 and 18, 453 km^2, respectively. The largest is comparable to the lake Ontario in Canada, which is 18,960 Km2. The generated cross sections show how relatively flat these palaeolakes are (Fig. 7). Palaeolakes A and B show a flat topography with some prominent depressions, including a straight one. The latter

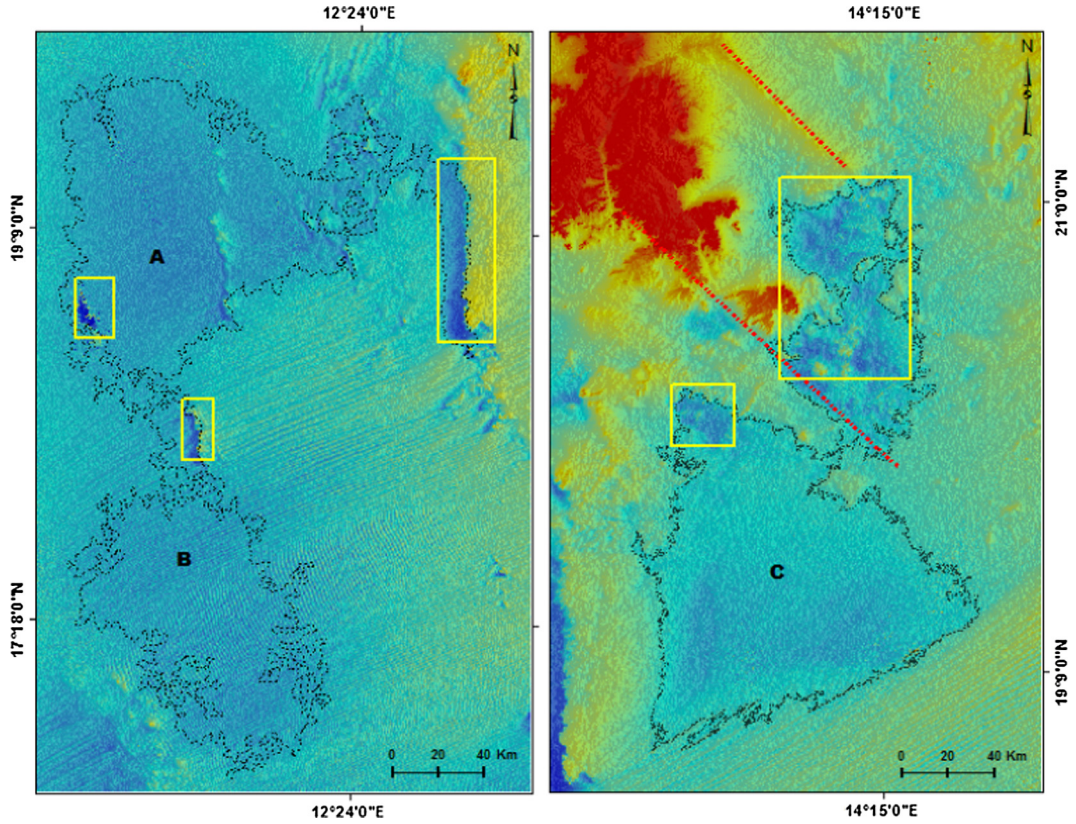

Fig. 8. SRTM data showing paleolakes A, B and C. Yellow boxes indicate the lowest areas within the flat lands. Note two main NW-SE faults dissecting Djado plateau that reach the northern part of palaeolake C.

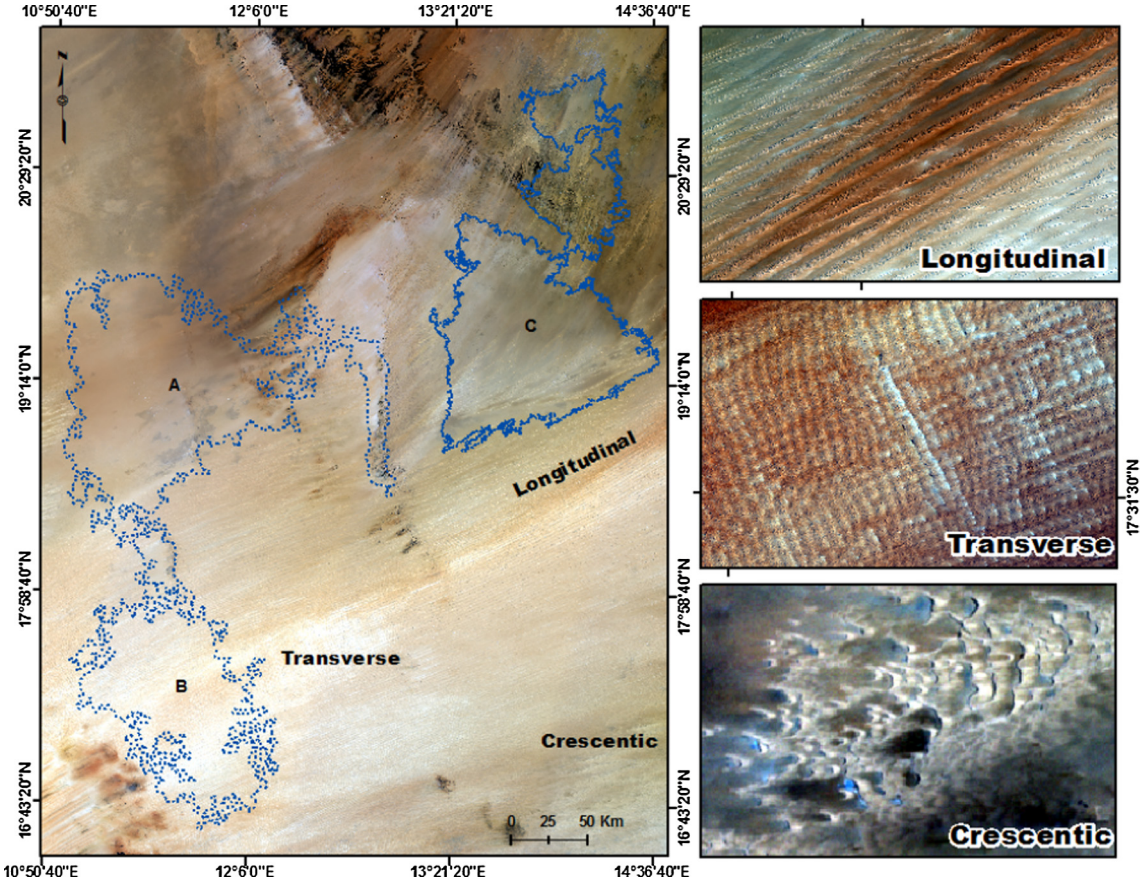

Fig. 9. Landsat images showing sand dunes emanating from southwestern Tibesti Mountain of north Chad. Most dunes form are either longitudinal or transverse. Within areas of vast accumulation of sand crescentic dunes abound.

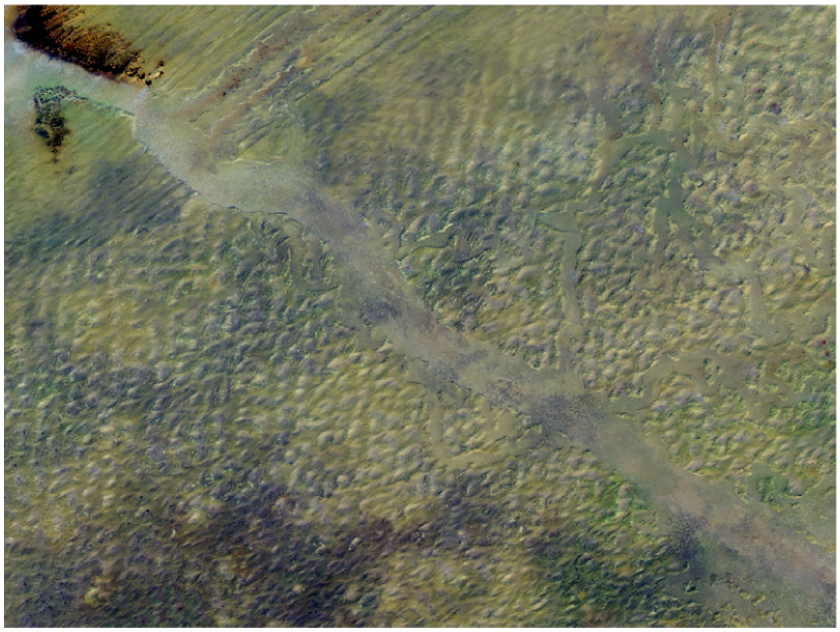

Fig. 10. Enlargement of a Landsat image, showing the removal of sand due to occasional passage of water through the channel of the Dillia stream.

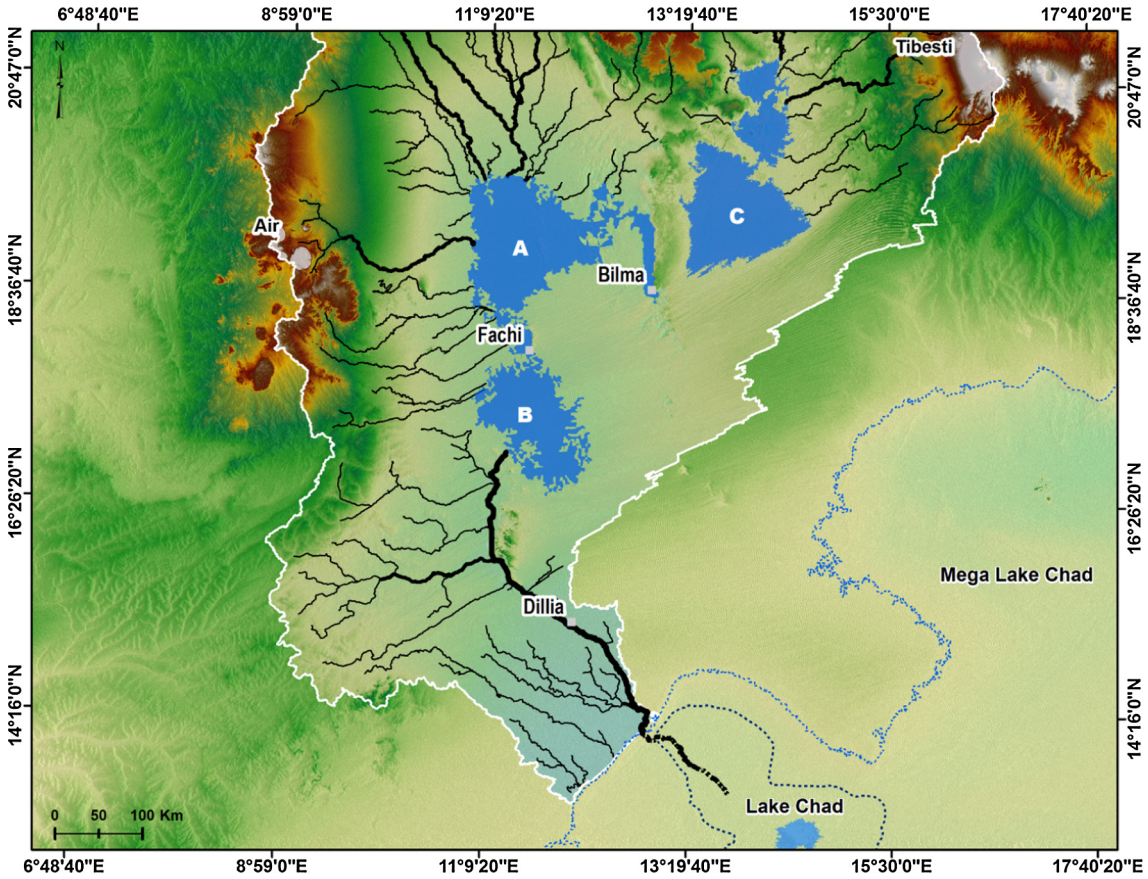

Fig. 11. Shows the connection between the identified three palaeolakes (A, B and C) and the lake of Chad through the Dillia stream.

hosts several villages, most probably due to the accumulation of surface water in the rainy seasons. Palaeolakes B and C show a relative homogenous topography. Fig. 8 shows the palaeolakes flattest areas, with small lakes highlighted by yellow boxes. There are pronounced NW-SE faults, which extend from Djado Plateau. These have dissected the northern part of palaeolake C (Fig. 8).

Along the present study area nearly all forms of sand dunes occur, indicating multiple transport mechanisms of various amount of sand. The latter was produces by water erosion during pluvial periods of the past, when the region was closer to the equator and received greater amount of rainfall (Abdelkareem and El-Baz, 2015). When the climate changed to dry, the wind

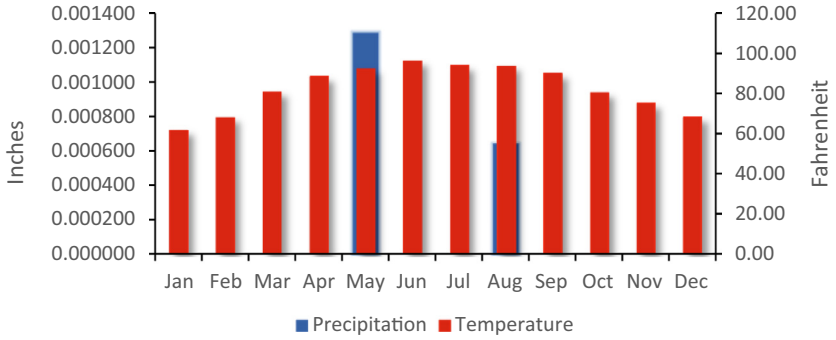

Fig. 12. Histogram showing the monthly average precipitation (inches) and temperature (Fahrenheit) from the Tibesti weather station in Chad (records of 2016).

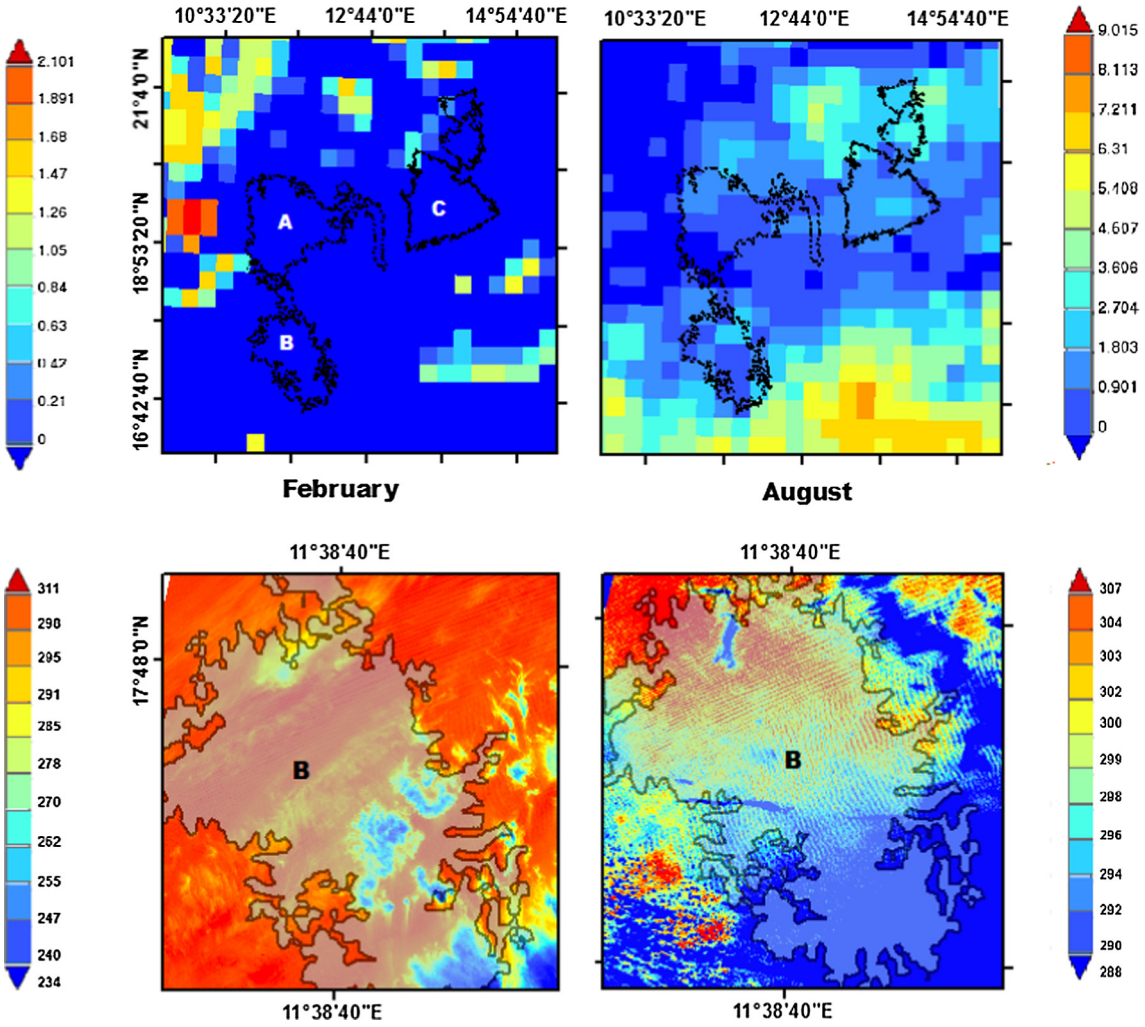

Fig. 13. Top: Average monthly precipitation map is in inches, from TRMM, showing the dry period, which corresponds to the month of February and the wet season of the month of August (right). Temperature in Kelvin (bottom) showing the agreement with precipitation data for the months of February and August, dark blue areas (left) correspond to clouds.

began to transport the sand and modify the topography. The wind came from the northeast and became gradually westerly (El-Baz, 1998).

The most distinct sand field emanated from the Tibesti Mountains of northern Chad to form longitudinal dunes in parallel bundles. To the south of these linear forms, transverse dunes occur in great amounts. These dunes accumulation mask the eastern border of the three lakes, particularly C and B. In areas of flat topography, particularly at the edges of larger dune accumulations, crescentic dunes abound, some with clear barchans shapes (Fig. 9). Those in the way of drainage lines are modified or removed by the occasional water action (Fig. 10). Fig. 11 shows the connection between the identified three palaeolakes and the Mega lake of Chad through the Dillia stream.

Daily precipitation records were obtained from January to December 2016 using TRMM data as well as historical records from

Tibesti weather station in Chad (Figs. 12 and 13). They show considerable rainfall fluctuation during the month of May, with a maximum average of 0.001290 inches, and in August, which reach 0.000645 inches. The remaining months are characterized by an absence of rain or negligible precipitation. Average temperatures show a minimum of 62° F for the month of January and a maximum average temperature of 97° F for the month of June (Fig. 12). Although the nearest climatological station to the study area was in Bilma, precipitation averages records from that station were not accurate and show higher temperatures than those recorded by Tibesti station. In contrast, precipitation averages from TRMM data show similar results to those of the Tibesti station. These indicate relative dryness during the month of February, while the most raining month is August (Fig. 12).

It is clear that the climate of Niger is variable, ranging from Saharan conditions in the northern half of the country to Sahelian climate in the south. The climate is characterized by two main seasons, the rainy period from June to September (although precipitation is relatively irregular), and the dry season from October to May. During the wet season the monsoon winds blow from the southwest to northeast dominating over most of the country. The dry season, however is characterized by the harmattan, which is a hot and dry wind (UNICEF, 2010).

The obtained results using the thermal data show an agreement with the averages precipitation data within the study area. The hottest month is February, while May and August are the coolest months. In addition, the obtained thermal results reveal the effect of the sediments in the study area, based on their heat conductivity and thermal inertia.

5. Conclusions

The shortage of fresh water in the Great Sahara makes any contribution to the potential locations of areas for groundwater accumulation is of great importance. Several researchers continue to investigate the potential of water resources through the desert. It is assumed that groundwater must exist as accumulations from many years of wetter climate when climate of North Africa was milder.

In this study, three distinct palaeolakes were identified from satellite image data and were properly mapped. The southern boundaries of these former marshlands have been modified by thick deposits of sand dunes, which accumulated during the prevailing arid conditions. These former palaeolakes received surface water from the surrounding highland. The latter include the Tibesti Mountain of northern Chad, the Ahaggar Plateau and Tassili-in-Ajjer of southeastern Algeria and the Air Mountain of northern Niger.

Water overflow of the southernmost lake led to the formation of a distinct drainage line named here Dillia Palaeoriver, which leads to the southwestern edge of the ancestral Megalake Chad. This stream would have contributed to increasing the level of water of the remnant Lake Chad during rainy seasons of the past. It must be stated, however, that these satellite images results require geophysical fieldwork to ascertain the interpretations as well as evaluate the potential of defining groundwater accumulation sites.

Precipitation and thermal data would need to be evaluated for a larger period of time to obtain more precise results; this is due to the fact that only records from one meteorological station were analyzed. Radar data revealed details in paleodrainage hidden and paleochannels in some areas. However, further analysis would have to be taken into consideration, because only C-band with two polarization direction (HH and VV) provided by sentinel-1 free data were analyzed. It is possible that longer wavelengths with different polarization would reveal more details due to the capability of radar data to penetrate sand surfaces.

This paper shows the benefits of using remote sensing data, both optical and radar, to map paleodrainage and palaeolakes over large arid and semi-arid areas. The identification of the new potential source of groundwater and near-surface water would benefit a large community that is in desperate need of water.

References

Abdelkareem, M., El-Baz, F., 2015. Regional view of Trans-African drainage system. J. Adv. Res. 6, 433–439.

African Development Bank 2012. Water Resources Mobilization and Development Project (Promovare). Republic of Niger. Project Appraisal Report. August 2012. p. 27.

ASETER GDEM Validation Team. 2011. ASTER Global Digital Elevation Model Version 2- Summary of Validation Results. NASA Land Processes Distributed Active Archive Center and the Joint Japan-US ASTER Science Team. p. 26.

Boos, W.R., Korty, R.L., 2016. Regional energy budget control of the intertropical convergence zone and application to mid-Holocene rainfall. Nat. Geosci. 9, 892–897. https://doi.org/10.1038/ngeo2833.

Brookfield, M.E., 2011. Aeolian process and features in cool climates. Geol. Soc. London Spec. Publ. https://doi.org/10.1144/SP354.16.

Choubert, G., Faure-Muret, A., Chanteux, P., Roche, G., 1987. International Geological Map of Africa, sheet 2, scale 1:5,000,000. U.N. Educ. Sci. Cult. Organ, Paris.

Costa-Cabral, M.C., Burges, S.J., 1994. Digital elevation model networks. (DEMON): a model of flow over hillslopes for computation of contributing and dispersal area. Water Resour. Res. 30 (6), 1681–1692. https://doi.org/10.1029/93WR03512.

Dai, A., 2011. Drought under global warming: a review. WIREs Clim. Change 2, 45–65. https://doi.org/10.1002/wcc.81.

Dilts, T.E., 2015. Flow accumulation for both positive and negative values toolbox for ArcGIS 10.1. University of Nevada Reno. Available at: http://www.arcgis.com/home/item.html?id=40d33968c44e4c9395c9c1ff1edd2bbe.

Drake, N.A., Blench, R.M., Armitage, S.J., Bristow, C.S., White, K.H., 2011. Ancient water courses and biogeography of the Sahara explain the peopling of the desert. Proc. Natl. Acad. Sci. U.S.A. 108 (2), 458–462.

El-Baz, F., 1998. Sand accumulation and groundwater in the eastern Sahara. Episodes. Int. Union Geol. Sci. 21 (3), 147–151.

Elmahdy, S.I., 2011. Hydromorphological mapping and analysis for characterizing Darfur Palaeolake, NW Sudan using remote sensing and GIS. Int. J. Geosci. 3, 25–36.

Elmahdy, S.I., Mohamed, M.M., 2013. Remote sensing and GIS applications of surface and near- surface hydromorphological features in Darfur region, Sudan. Int. J. Remote Sens. 34, 4715–4735.

Fabre, J., Mainguet, M., 1991. Continental sedimentation and palaeoclimates in Africa during the Gondwanian Era (Cambrian to Lower Cretaceous): the importance of wind action. J. African Earth Sci. (and the Middle East). 12, 107–115.

Fairfield, J., Leymarie, P., 1991. Drainage networks from grid elevation models. Water Resour. Res. 27 (5), 709–717. https://doi.org/10.1029/90WR02658.

Forkuor, G., Maathuis, B.M., 2012. Comparison of SRTM and ASTER derived digital elevation models over two regions in Ghana: Implications for hydrological and environmental modeling. In: Piacentini, T., Miccadei, E. (Eds.), Studies on Environmental and Applied Geomorphology, InTech. 10.5772/28951. ISBN 978-953-51-0361-5. pp. 219–240.

Fujisada, H., Bailey, G.B., Kelly, G.G., Hara, S., Abrams, M.J., 2005. ASTER DEM performance. IEEE Trans. Geosci. Remote Sens. 43, 2707–2714.

Gaber, A., Ghoneim, E., Khalaf, F., El-Baz, F., 2009. Delineation of paleolakes in arid regions using remote sensing and GIS. J. Arid Environ. 73, 127–134.

Gaber, A., Soliman, F., Koch, M., El-Baz, F., 2015. Using full-polarimetric SAR data to characterize the surface sediments in desert areas: a case study in El-Gallaba Plain, Egypt. Remote Sens. Environ. 16, 11–28.

Gasse, F., 2000. Hydrological changes in the African tropics since the Last Glacial Maximum. Quatern. Sci. Rev. 19 (1–5), 189–211.

Ghoneim, E., El-Baz, F., 2007. Radar topography data reveal drainage relics in the eastern Sahara. Int. J. Remote Sens. 28, 5001–5018.

Ghoneim, E., Robinson, C., El-Baz, F., 2007. DEM-optical-radar data integration for palaeohydrological mapping in the northern Darfur, Sudan: implication for groundwater exploration. Int. J. Remote Sens. 28 (22), 5001–5018.

Ghoneim, E., Arnell, N.W., Foody, G.M., 2002. Characterizing the flash flood hazards potential along the Red Sea Coast of Egypt. In: Snorasson, A., Finnsdóttir, H.P., Moss, M.E. (Eds.), The Extremes of the Extremes: Extraordinary Floods. IAHS Publishers, pp. 211–216.

Goudie, A.S., 2002. Great Warm Deserts of the World: Landscape and Evolution. Oxford University Press. 444.

Hensley, S., Mungy, R., Rosen, P., 2001. In Interferometric Synthetic Aperture Radar (IFSAR), Digital Elevation Model technologies and applications: The DEM Users Manual. In: Maune, D. (Ed.). pp. 143–206 (Bethesda, MD: American Society for Photogrammetry and Remote Sensing).

Hirt, C., Filmer, M.S., Featherstone, W.E., 2010. Comparison and validation of the recent freely available ASTER-GDEM ver1, SRTM ver4. 1 and GEODATA DEM-9S ver3 digital elevation models over Australia. Aust. J. Earth Sci. 57 (3), 337–347.

Jenson, S., Dominique, J., 1988. Extracting topographic structure from digital elevation data for geographical information system analysis. Photogram. Eng. Remote Sens. 54 (11), 1593–1600.
Jolly, D., Harrison, S.P., Damnati, B., Bonnefille, R., 1998. Simulated climate and biomes of Africa during the late quaternary: comparison with pollen and lake status data. Quatern. Sci. Rev. 17 (6–7), 629–657.
Kobrick, M., 2006. On the toes of giants: How SRTM was born. Photogram. Eng. Remote Sens. 72 (3), 206–210.
Larrasoaña, J.C., Roberts, A.P., Rohling, E.J., 2013. Dynamics of green Sahara periods and their role in Hominin evolution. PLOS ONE 8 (10), e76514.
Leblanc, M., Favreau, G., Tweed, S., Leduc, C., Razack, M., Morfor, L., 2007. Remote sensing for groundwater modelling in large semiarid areas: Lake Chad Basin, Africa. Hydrogeological J. 15 (1), 97–100.
Lockwood, M., Kothari, A., Worboys, G., 2006. Managing Protected Areas: A Global Guide. ISBN: 978-1-84407-303-0. Earthscan UK. Case Study 1.10 Aïr and Ténéré Natural Reserves.
Luedeling, E., Siebert, S., Buerkert, A., 2007. Filling the voids in the SRTM elevation model—a TIN-based delta surface approach. ISPRS J. Photogram. Remote Sens. 62 (4), 283–294. https://doi.org/10.1016/j.isprs.jprs.
Mainguet, M., 1978. The influence of trade winds, local air masses and topographic obstacles on the aeolian movement of sand particles and the origin and distribution of dunes and ergs in the Sahara and Australia. Geoforum 9 (1), 17–28.
Mainguet, M., 1984. A classification of dunes based on eolian dynamics and the sand budget. In: El-Baz, F. (Ed.), Deserts and Arid Lands. Martinus NijhoM Publishers, The Hague, pp. 31–58.
Mainguet, M., Chemin, M.-C., 1983. Sand seas of the Sahara and Sahel: an explanation of their thickness and sand dune type by the sand budget principle. Dev. Sedimentol. 38, 353–363.
Mainguet, M., Callot, Y., 1978. L'erg de Dillia-Bilma (Tchad-Niger). Contribution a la connaissance de la dynamique des ergs et des dunes des zones arides chaudes. Memoires ed Documents. Novuelle Serie. pp. 18:1-184.
Marks, D., Dozier, J., Frew, J., 1984. Automated basin delineation from digital elevation data. GeoProcessing 2, 299–311.
Martz, L.W., Garbrecht, J., 1992. Numerical definition of drainage network and subcatchment areas from digital elevation models. Comput. Geosci. 18 (6), 747–761.
Maxwell, T.A., Issawi, B., Haynes, C.V., 2010. Evidences for Pleistocene lakes in the Tushka region, south Egypt. Geol. Soc. America 32 (12), 1135–1138.
Nasa, J.P.L., 2013. NASA Shuttle Radar Topography Mission Global 1 arc second. NASA LP DAAC. https://doi.org/10.5067/MEaSUREs/SRTM/SRTMGL1.003.
Nikolakopoulos, K.G., Kamaratakis, E., Chrysoulaki, N., 2006. SRTM vs ASTER elevation products. Comparison for two regions in Crete, Greece. Int. J. Remote Sens. 27 (21), 4819–4838.
O'Callaghan, J.F., Mark, D.M., 1984. The extraction of drainage networks from digital elevation data computer vision. Graphics Image Process. 28 (3), 323–344.
Paillou, P., 2017. Mapping Palaeohydrography in Deserts: Contribution from Space-Borne Imaging Radar. Water 9 (3), 194. https://doi.org/10.3390/w9030194.
Paillou, P., Grandjean, G., Baghdadi, N., Heggy, E., August-Bernex, T., Achache, J., 2003. Subsurface imaging in central-southern Egypt using low frequency radar: Bir Safsaf revisited. IEEE Trans. Geosci. Remote Sens. 41 (7), 1672–1684.
Persits, F., Ahlbrandt, T., Tuttle, M., Charpentier, R., Brownfield, M., Takahashi, K., 2002. Oil and gas fields and geologic provinces of Africa. Ver 2.0. USGS Open File report 97-470 A. British Geological Survey. Niger Geology.png. USGS.
Robinson, C., El-Baz, F., Al-Saud, T., Jeon, S., 2006. Use of radar data to delineate palaeodrainage leading to the Kufra Oasis in the Eastern Sahara. J. Afr. Earth Sci. 44, 229–240.
Robinson, C.A.F., El-Baz, M., Ozdogan, M., Ledwith, D Blanco, Oakley, S., Inzana, J., 2000. Use of radar data to delineate palaeodrainage flow directions in the Selima Sand Sheet, Eastern Sahara. Photogram. Eng. Remote Sens. 66 (6), 745–753.
Rossi, A.P., Marinangeli, L., 2004. The first terrestrial analogue to Martian dust devil tracks found in Ténéré Desert, Niger. Geophys. Res. Lett. 31, L06702. https://doi.org/10.1029/2004GL019428.
Schaber, G., Mccauley, J., Breed, C., 1997. The use of multifrequency and polarimetric SIR– C/X–SAR data in geologic studies of Bir Safsaf, Egypt. Remote Sens. Environ. 59, 337–363.
Shao, Y., 2001. Physics and modeling of wind erosion. Series: Atmospheric and Oceanographic Sciences Library, vol. 23, pp. 408.
Skinner, C.B., Poulsen, C.J., 2016. The role of fall season tropical plumes in enhancing Saharan rainfall during the African Humid Period. Geophys. Res. Lett. 43, 349–358.
Skonieczny, C., Paillou, P., Bory, A., Bayon, G., Biscara, L., Crosta, X., Eynaud, F., Malaize, B., Revel, M., Aleman, N., Barusseau, J.-P., Vernet, R., Lopez, S., Grousset, F., 2015. African humid periods triggered the reactivation of a large river system in Western Sahara. Nat. Commun. 6, 8751. https://doi.org/10.1038/ncomms9751.
Slater, J.A., Heady, B., Kroenung, G., Curtis, W., Haase, J., Hoegemann, D., Shockley, C., Kevin, T., 2009. Evaluation of the New ASTER Global Digital Elevation Model. Available online at: http://earth-info.nga.mil/GandG/elevation/ (accessed 24 June 2011).
Tarboton, D.G., 1997. A new method for the determination of flow directions and upslope areas in grid digital elevation models. Water Resour. Res. 33 (2), 309–319.
Tierney, J.E.F.S.R., Pausata, F.S.R., deMenocal, P.B., 2017. Rainfall regimes of the Green Sahara. Sci. Adv. 3 (1), e1601503. https://doi.org/10.1126/sciadv.1601503.
UNICEG, 2010. Etude de faisabilité des forages manuels identification des zones potentiellement favorables. Republique du Niger Ministere de l'Eau, de L'Environnement et de la Lutte Contre Le Desertification. pp. 23.
Vassolo, S., 2012. Groundwater need assessment Lake Chad Basin, prepared by BGR, 26 p (PDF, 1 MB).
Warren, A., 1971. Dunes in the Ténéré Desert. Geogr. J. 137, 458–4691.
Wilson, I.G., 1973. Ergs. Sed. Geol. 10 (2), 77–106.
Zhao, G.J., Gao, J.F., Tian, P., Tian, K., 2009. Comparison of two different methods for determining flow direction in catchment hydrogeological modeling. Water Sci. Eng. 2 (4), 1–15. https://doi.org/10.3882/j.issn.1674-2370.2009.04.001.